Chinese Chemical Letters 35 (2024) 108535

Contents lists available at ScienceDirect

Chinese Chemical Letters

journal homepage: www.elsevier.com/locate/cclet

De novo design of highly efficient type-I photosensitizer based on π-conjugated oligomer for photodynamic eradication of multidrug-resistant bacterial infections

Qi Zhao[a,b,1], Guangchao Qing[c,1], Jie Yu[b], Ying Liu[b], Jianliang Shen[a], Yang Luo[c,d,*], Xingjie Zan[a,*], Shengliang Li[b,*]

[a] State Key Laboratory of Ophthalmology, Optometry and Vision Science, School of Ophthalmology and Optometry, School of Biomedical Engineering, Wenzhou Medical University; Wenzhou Institute, University of Chinese Academy of Sciences; Oujiang Laboratory (Zhejiang Lab for Regenerative Medicine, Vision and Brain Health), Wenzhou 325001, China
[b] College of Pharmaceutical Sciences, Soochow University, Suzhou 215123, China
[c] Center of Smart Laboratory and Molecular Medicine, School of Medicine, Chongqing University, Chongqing 400044, China
[d] College of Life Science and Laboratory Medicine, Kunming Medical University, Kunming 650050, China

ARTICLE INFO

Article history:
Received 13 February 2023
Revised 1 May 2023
Accepted 4 May 2023
Available online 9 May 2023

Keywords:
Photodynamic therapy
Antibacterial
Type-I photosensitizers
Multidrug-resistant bacteria
Conjugated oligomers

ABSTRACT

Traditional photosensitizers show limited singlet oxygen generation in hypoxic infection lesions, which greatly suppress their performance in antibacterial therapy. Meanwhile, there still is lack of feasible design strategy for developing hypoxia-overcoming photosensitizers agents. Herein, radical generation of π-conjugated small molecules is efficiently manipulated by an individual selenium (Se) substituent. With this strategy, the first proof-of-concept study of a Se-anchored oligo (thienyl ethynylene) (**OT-Se**) with high-performance superoxide radical ($O_2^{\bullet-}$) and hydroxyl radical ($^{\bullet}OH$) generation capability is present, and achieves efficient antibacterial activities towards the clinically extracted multidrug-resistant bacteria methicillin-resistant *S. aureus* (MRSA) and carbapenem-resistant *E. coli* (CREC) at sub-micromolar concentration under a low white light irradiation (30 mW/cm^2). The water-dispersible **OT-Se** shows a good bacteria-anchoring capability, biocompatibility, and complete elimination of multidrug-resistant bacteria wound infection *in vivo*. This work offers a strategy to boost type-I photodynamic therapy (PDT) performance for efficient antibacterial treatments, advancing the development of antibacterial agents.

Numerous pathogenic bacterial infections seriously threaten human health throughout the world [1]. It is even worse that bacterial infections with a strong resistance against conventional antibiotics have increased dramatically in the past decade [2–5]. As noted by the World Health Organization (WHO), multidrug-resistant (MDR) bacteria have become the top 10 of worldwide public health crises and are a serious global threat to human health [6]. Thus, there is a timely urgent need to develop a new approach with resistance-free capability for high-performance bacterial eradication.

Given the failure of antibiotics to fight against various resistant bacterial infections, nonantibiotic strategies have been closely on the rise over the past few years to overcome these inefficiencies in treating various drug-resistant bacterial infections [7–13]. Among these nonantibiotic methods, photodynamic therapy (PDT) has received increasing concern due to its advantages of high spatiotemporal precision, ignorable drug resistance, and broad antibacterial spectrum [14–19]. However, most existing PDT agents mainly generate singlet oxygen ($^1O_2$) by commonly employing a type-II PDT process, which is known as an oxygen-dependent modality and whose applications have been largely limited by the natural hypoxic conditions of infection and biofilms [20–22]. In contrast, type-I PDT agents employing electrons to generate radical species such as superoxide radicals ($O_2^{\bullet-}$) and hydroxyl radicals ($^{\bullet}OH$) show much less dependency on the oxygen level [23–27]. Given the potential of type-I PDT, a handful of type-I photosensitizers (PSs) have been explored for antibacterial applications in recent years [22,23,28-30]. However, the radical generation efficiency of reported type-I PSs is still at a relatively low level, and the feasible molecular design for type-I PDT agents is still unknown until now.

* Corresponding authors.
E-mail addresses: luoy@cqu.edu.cn (Y. Luo), xjzan2000@hotmail.com (X. Zan), lishengliang@suda.edu.cn (S. Li).
[1] These authors contributed equally to this work.

https://doi.org/10.1016/j.cclet.2023.108535
1001-8417/

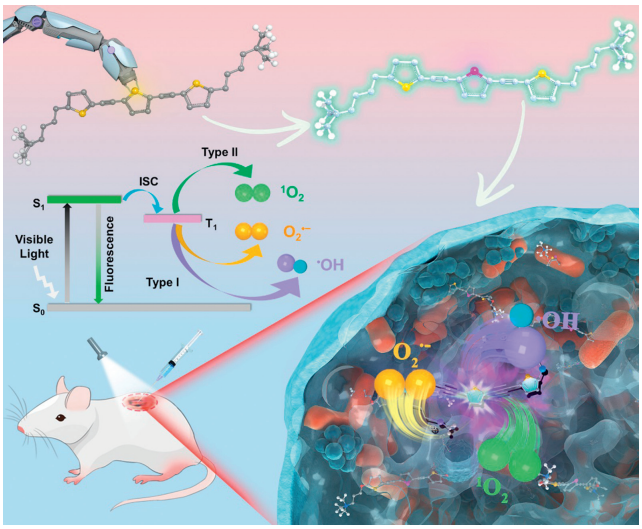

Scheme 1. Schematic illustration of atomic manipulation of conjugated oligomers for eradicating multidrug-resistant bacterial infection.

Conjugated oligomers that consist of a few similar conjugated units were characterized with strong electron-delocalized and tunable optoelectronic properties. Recent advances in the fields of organic photovoltaics (OPVs) [31,32], organic light-emitting diodes (OLEDs) [33,34], and organic field-effect transistors (OFETs) [35,36] have led to the development of conjugated oligomers. Taking advantage of their light-harvesting and light-amplifying capabilities, conjugated oligomers have also been widely used for biomedical applications, mainly biosensors, imaging, and phototherapy [37–41]. In recent years, conjugated oligomers have been successfully explored as antibacterial PSs due to their high singlet oxygen generation [42–46]. However, these reported conjugated oligomers mainly concentrate on the development of type-II PDT, which generally restricted by oxygen level in lesion.

In this work, we developed a conjugated oligomer photosensitizer **OT-Se** to efficiently boost radical generation capability for eradicating multidrug-resistant bacterial infection (Scheme 1). The molecular design originates from oligo(thienyl ethynylene) (**OT-S**), which possesses good visible light-harvesting capability with high-performance $^1O_2$ generation [39]. *Via* individual selenium (Se) anchoring, the $O_2^{\bullet-}$ and ·OH radical yields of **OT-Se** were efficiently enhanced through the type-I mechanism. In addition, cationic quaternary ammonium salts were conjugated into both ends of **OT-Se** to provide a reliable bacterial membrane-anchoring function. Both *in vitro* and *in vivo* investigations indicated that **OT-Se** serves as a type-I photosensitizer that can photodynamically kill antibiotic-resistant bacteria and achieve complete elimination of wound infection with good biocompatibility. Thus, our study offers a reliable molecular strategy for developing high-performance type-I PDT agents and holds great potential in bacterial infection treatments.

The oligo(thienyl ethynylene)s, **OT-S** and **OT-Se**, were synthesized according to a synthetic route, as shown in Fig. S1 (Supporting information). **OT-S** and **OT-Se** were synthesized *via* Sonogashira coupling and then anchored with a cationic group quaternary ammonium salt in the two terminals. To achieve a heavy-atom effect, a strong acceptor selenophen was introduced to replace the in-between thiophene of **OT-S** for building the **OT-Se** compound (Fig. 1a). The molecular structures of OTs and their intermediates were characterized with nuclear magnetic resonance (NMR) spectroscopy and high-revolution mass spectrometry (Figs. S2–S15 in Supporting information). Both **OT-S** and **OT-Se** have good water solubility and show broad absorption from 300 nm to 450 nm with typical blue-green fluorescence emission in the range of 420–650 nm (Fig. 1b). Compared with **OT-S**, **OT-Se** shows an approximate 20 nm bathochromic shift in the absorption and emission peaks, with weaker fluorescence intensity under ultraviolet (UV) lamp irradiation (Fig. S16 in Supporting information).

The total reactive oxygen species (ROS) generation performance of OTs was evaluated by measuring the variation in the emission spectra of 2,7-dichlorodihydrofluorescein (DCFH, an ROS indicator) upon white light exposure (400–700 nm, 1 mW/cm^2). As shown in Fig. 1c, the 525 nm fluorescence of DCFH treated with **OT-S** and **OT-Se** shows an obvious increase with the time of white light irradiation. Importantly, **OT-Se** shows a more remarkable fluorescence increase than **OT-S**, implying that **OT-Se** has a higher total ROS generation capability than **OT-S**. We then investigated the singlet oxygen ($^1O_2$) generation capability of **OT-S** and **OT-Se** using 1,3-diphenylisobenzofuran (DPBF, a $^1O_2$ indicator) and methylene blue (MB, a PS standard) and found that the relative $^1O_2$ quantum yields (Φ) of **OT-Se** ($\Phi = 0.57$) and **OT-S** ($\Phi = 0.56$) were approximately similar and had comparable $^1O_2$ capability towards MB (Fig. 1d and Fig. S17 in Supporting information). To further explore the type-I photochemical reaction of OTs, the superoxide radical ($O_2^{\bullet-}$) and hydroxyl radical (·OH) generation performance was investigated by dihydrorhodamine 123 (DHR123, an $O_2^{\bullet-}$ indicator) and hydroxyphenyl fluorescein (HPF, a ·OH indicator), respectively. As shown in Figs. 1e–g, upon 320 s of white light irradiation (50 mW/cm^2), the $O_2^{\bullet-}$ and ·OH generation capability of **OT-Se** is 1.5 times and 1.9 times as much as that of **OT-S**, respectively. These results demonstrated that incorporating selenium atoms into OTs would augment the intersystem crossing (ISC) efficiency and type-I photochemical reaction for radical species generation [47], as summarized in Fig. 1h. The enhancement in radical species generation of **OT-Se** holds great potential in hypoxia-associated antibacterial and anti-infection applications.

Membrane anchoring can endow photosensitizers with local enrichment in the bacterial cell membrane, which is beneficial for ROS-driven lipid peroxidation and ultimately leads to efficient bacterial death. **OT-Se** is a typical "end-only" conjugated oligomer with hydrophilic quaternary ammonium salt structures on both ends of the molecule and hydrophobic aromatic acetylene structure in the backbone, thus holding great potential for membrane anchoring. To investigate the interaction between **OT-Se** and bacteria, the change in zeta potential of *E. coli* before and after **OT-Se** treatment was measured (Fig. S18 in Supporting information). The results show that the negative zeta potential of *E. coli* (−46.8 mV) became positive (+58.9 mV) after 1 min incubation of **OT-Se** (20 μmol/L) in saline, with a typical positive correlation with the **OT-Se** concentration, suggesting good bacteria-binding capability. Confocal laser scanning microscopy (CLSM) was further employed to visualize the bacteria-binding performance. As shown in Fig. 1i, green-fluorescent **OT-Se** could first anchor to the bacterial membrane and then quickly enter the bacterial cytoplasm within 100 s of interaction. Z-series scanning of CLSM further confirmed that **OT-Se** would completely stain the whole bacteria. These results indicate that **OT-Se** can rapidly anchor to bacteria and provide a chance for efficient bacterial killing.

Inspired by the good ROS generation capability of **OT-Se**, we next used the standard plate colony-counting method to evaluate the antibacterial activity of **OT-Se** towards the Gram-negative bacterium *E. coli* and the Gram-positive bacterium *S. aureus*. As shown in Fig. S19 (Supporting information), the death percentage of **OT-Se**-treated *E. coli* and *S. aureus* increased significantly with increasing **OT-Se** concentration upon 30 mW/cm^2 white light irradiation for 30 min, while **OT-Se** under dark conditions exhibited relatively low antibacterial activities against *E. coli* and *S. aureus.* Furthermore, the antibacterial activities of **OT-Se** against *E. coli* and *S. aureus* showed irradiation time-dependent profiles (Fig.

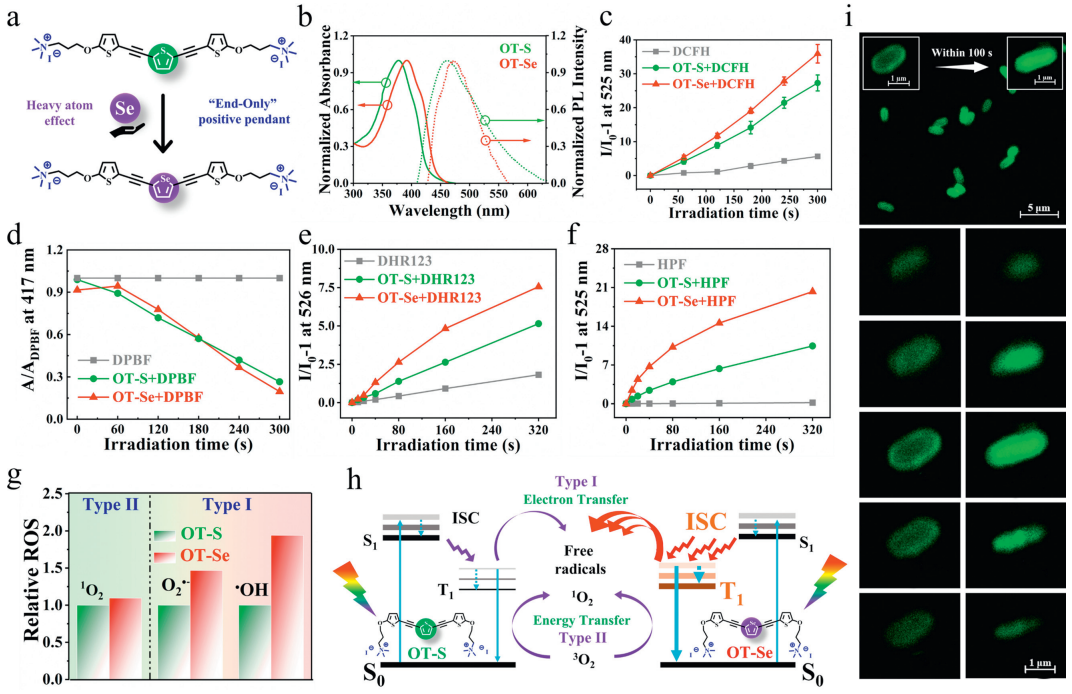

Fig. 1. Characterizing ROS generation and membrane anchoring. (a) Molecular structures of OTs. (b) Normalized UV-vis absorption and emission spectra of **OT-Se** (red) and **OT-S** (green). (c) Total ROS generation of **OT-Se** and **OT-S** at the same concentration using DCFH as an ROS indicator (λ_{ex} = 488 nm, λ_{em} = 525 nm). (d) $^1O_2$ generation of **OT-Se** and **OT-S** using DPBF as an indicator. $O_2^{\bullet-}$ (e) and $^{\bullet}OH$ (f) generation of **OT-Se** and **OT-S** using DHR 123 and HPF as indicators, respectively. (g) Comparison of **OT-Se** and **OT-S** in type-I and type-II ROS generation. (h) Schematic illustration of the ISC pathway for **OT-Se** and **OT-S**. (i) CLSM images of *E. coli* treated with **OT-Se** within different incubation times and focus planes. The scale bar in the top image is 5 μm and the other images are 1 μm.

S20 in Supporting information). Notably, the minimum bactericidal concentration (MBC) of **OT-Se** against *S. aureus* and *E. coli* was measured to be approximately 80 nmol/L and 2.5 μmol/L, respectively, suggesting that **OT-Se** has relatively high antibacterial activity compared with the reported PDT agents. In contrast, the heavy-atom-free **OT-S** showed relatively weak antibacterial activity against the two bacteria (Fig. S21 in Supporting information). The results demonstrated that the enhanced type-I PDT activity of **OT-Se** can afford highly efficient antibacterial capability against both Gram-negative bacteria and Gram-positive bacteria.

To further confirm the antibacterial activity, we performed live/dead staining to visualize the survival condition before and after **OT-Se** treatment. As shown in Fig. S22 (Supporting information), both **OT-Se**-treated *E. coli* and *S. aureus* display obvious red and orange fluorescence, while the bacteria treated with white light irradiation without **OT-Se** show almost completely green fluorescence, indicating that the photodynamic effect of **OT-Se** can induce efficient death towards *E. coli* and *S. aureus*. Next, scanning electron microscopy (SEM) was performed to evaluate the morphology change of bacteria after **OT-Se** treatment. Both *E. coli* and *S. aureus* treated with light irradiation in the absence of **OT-Se** had intact surfaces and morphologies (Fig. S23 in Supporting information). However, after **OT-Se** treatment plus light irradiation, the cell membranes of the two bacterial strains were seriously destroyed, and showed a certain extent of collapse and punching, thus indicating the interaction of the localized photodynamic effect of **OT-Se** towards bacteria.

It is widely known that multidrug-resistant bacteria and their infections are the greatest challenges in the clinic and annually cause numerous deaths throughout the world. At present, global scientists in the community of chemistry, pharmaceutical science, and biomedicine are committing themselves to exploring new methods or tracts for overcoming antibiotic resistance problems. Next, we systematically investigated the antibacterial activity of **OT-Se** against the clinically isolated multidrug-resistant bacteria methicillin-resistant *S. aureus* (MRSA) and carbapenem-resistant *E. coli* (CREC). As shown in Fig. 2, approximately 94% of MRSA is killed at 140 nm of **OT-Se**, and 2.5 μmol/L of **OT-Se** can kill more than 99.5% of CREC upon 30 mW/cm^2 white light irradiation. As noted, the anti-MRSA activity of **OT-Se** was nearly 17.8 times greater than the anti-CREC capability, suggesting relatively high MRSA-specific antibacterial activity. In contrast, **OT-Se** has weak antibacterial activities against the two bacteria without light irradiation (Fig. S24 in Supporting information). The growth curve experiment of MRSA and CREC further confirmed the highly efficient antibacterial results of **OT-Se** under illumination (Fig. S25 in Supporting information). The live/dead staining assay also confirms the highly efficient anti-MRSA and anti-CREC performance of plate-counting experiments. Moreover, SEM and TEM images verified the destructive effect of **OT-Se** on the cell membrane of MRSA and CREC bacteria through localized ROS generation (Fig. 2 and Fig. S26 in Supporting information). These above results suggest that biocompatible **OT-Se** with multi-ROS generation has highly efficient antibacterial activity against the multidrug-resistant bacteria MRSA and CREC and holds great potential for eradicating multidrug-resistant bacterial infections.

Motivated by the good *in vitro* activities against the multidrug-resistant bacteria CREC and MRSA, we further evaluated the *in vivo* antibacterial performance on a CREC and MRSA infection model of mouse skin (Fig. 3a). All animal experiment protocols were approved by the National Center for Nanoscience and Technology's Institutional Animal Care and Use Committee. With **OT-Se** treatment plus 30 min irradiation with white light, both CREC- and MRSA-infected wounds showed obvious disappearance of pyosis, and 98% of skin wounds healed after 10 days of treatment (Figs. 3b and e). In contrast, phosphate buffer saline (PBS) and **OT-Se** alone had relatively slow wound healing performance (60% for PBS; 75% for **OT-Se** alone) and maintained a slight inflammation

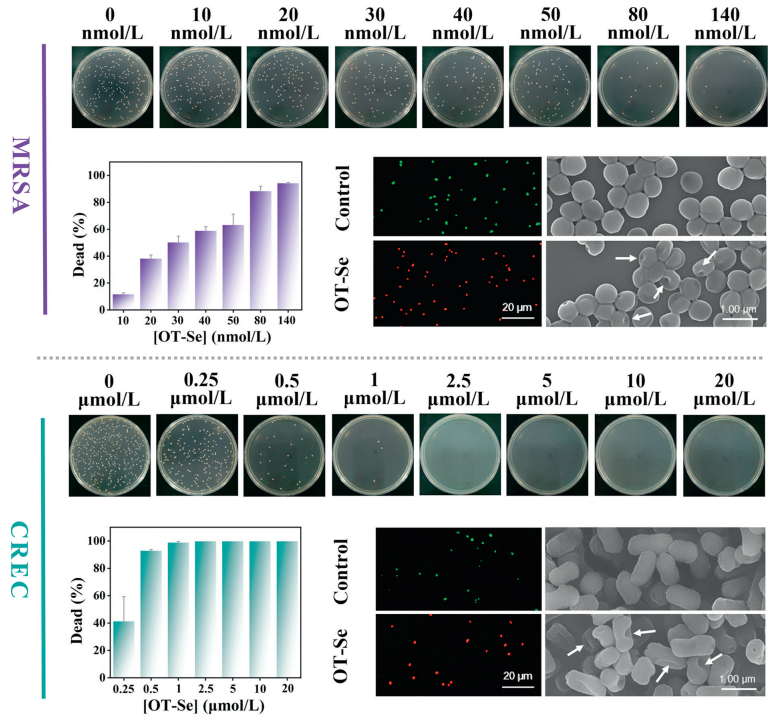

Fig. 2. *In vitro* antibacterial activity of **OT-Se** against multidrug-resistant bacteria upon white light irradiation (30 mW/cm^2) and live/dead staining (scale bar = 20 μm) and SEM images (scale bar = 1 μm) of MRSA and CREC after various treatments.

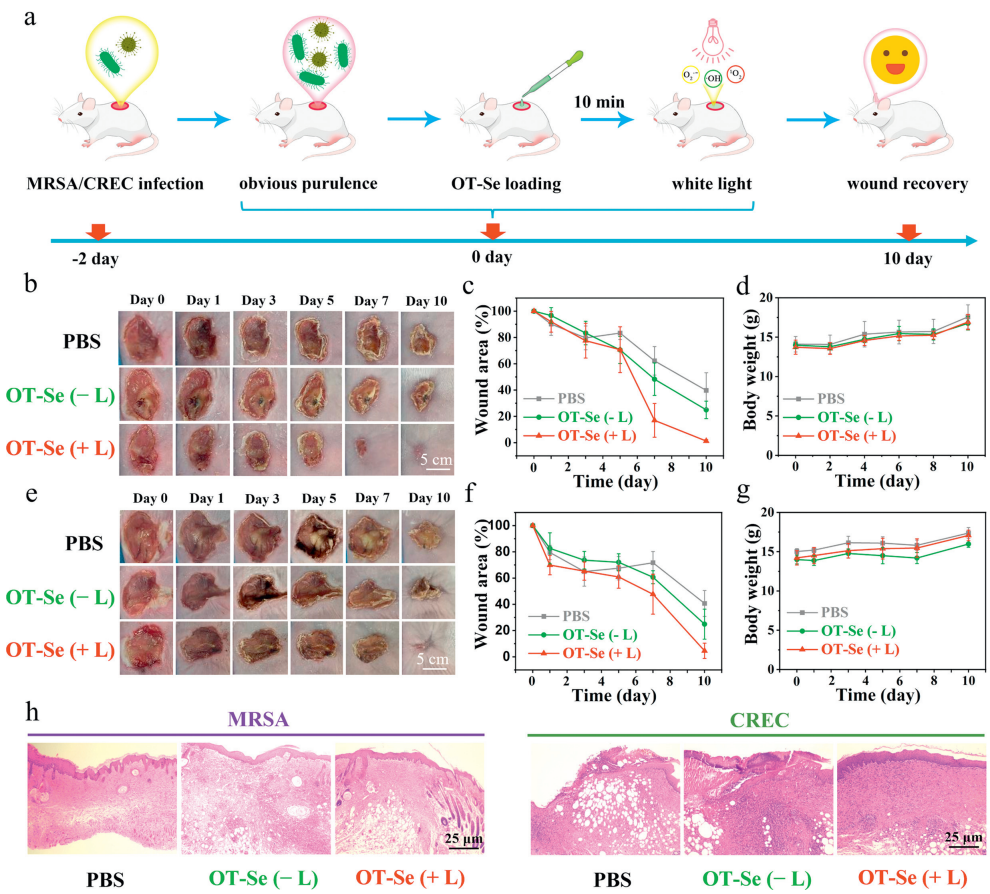

Fig. 3. *In vivo* antibacterial photodynamic therapy. (a) Schematic illustration of **OT-Se**-treated bacteria-infected mice. Wound images of MRSA (b) and CREC (e) infection during the different treatments (scale bar = 5 cm). Area quantification of MRSA (c) and CREC (f) infection regions. Weight change of MRSA-infected (d) and CREC-infected (g) mice in the period of treatment. (h) H&E images of the sectioned wound tissue (200×) after 10 days of treatment. Scale bar = 25 μm.

phenomenon. The macroscopic area of the infection wound further confirmed the high-performance antibacterial and wound healing capabilities (Figs. 3c and f). Hematoxylin and eosin (H&E) images of wound tissue demonstrate that **OT-Se** with light irradiation has more preferable skin repair and regrowth than the other two control groups (Fig. 3h and Fig. S27 in Supporting information). These results suggest that **OT-Se**-based PDT can efficiently eradicate multidrug-resistant bacterial infection to accelerate wound healing.

In vitro cytotoxicity experiments were conducted on normal cells NIH-3T3 and demonstrated that **OT-Se** shows negligible cytotoxicity towards NIH-3T3 at concentrations of 10 μmol/L, indicating good biocompatibility (Fig. S28 in Supporting information). The biosafety of **OT-Se** was evaluated by monitoring the weight change of mice after 10 days of treatment. No noticeable weight changes were observed in **OT-Se**-treated mice (Figs. 3d and g). In addition, H&E staining of the main organs showed nearly negligible inflammatory lesions and organ damage after 10 days of treatment, suggesting that **OT-Se** has good *in vivo* biocompatibility and biosafety (Fig. S29 in Supporting information).

In summary, we showed notably boosted radical generation in conjugated oligomers by anchoring a selenium substituent in the backbone and demonstrated their antibacterial infection performances against multidrug-resistant bacteria at sub-micromolar concentrations. Through the selenium substituent, **OT-Se** has a red-shifted absorption but lower fluorescence emission compared to OT-S. More importantly, the $O_2^{\bullet-}$ and $^{\bullet}OH$ radical generation of **OT-Se** was boosted to be 1.5 times and 1.9 times as much as that of OT-S, respectively, indicating the reliable enhancement effect on the type-I PDT. Due to their fast bacterial anchoring, **OT-Se** can be used as a type-I photosensitizer to photodynamically kill the clinically extracted antibiotic-resistant bacteria CREC and MRSA at extremely low concentrations. We also demonstrate that **OT-Se** can successfully eradicate CREC and MRSA bacterial infection and afford efficient wound healing with good *in vivo* biocompatibility. Our investigation has demonstrated the great promise of **OT-Se** as a type-I PDT agent for clinical antibacterial applications.

Declaration of competing interest

The authors declare that they have no known competing financial interests or personal relationships that could have appeared to influence the work reported in this paper.

Acknowledgments

This work was financially supported by the National Natural Science Foundation of China (Nos. 82125022, 82072383, 31800833, 21977081, 52173135 and 22207024), Zhejiang Provincial Natural Science of Foundation of China (No. LZ19H180001), Wenzhou Medical University (No. KYYW201901), and University of Chinese Academy of Science (Nos. WIBEZD2017001-03 and WIUCASYJ2020001).

Supplementary materials

Supplementary material associated with this article can be found, in the online version, at doi:10.1016/j.cclet.2023.108535.

References

[1] F. Werdin, M. Tenenhaus, H.O. Rennekampff, Lancet 372 (2008) 1860–1862.
[2] M. Baym, L.K. Stone, R. Kishony, Science 351 (2016) aad3292.
[3] C. Willyard, Nature 543 (2017) 15.
[4] X. Li, S. Lee, J. Yoon, Chem. Soc. Rev. 47 (2018) 1174–1188.
[5] Y. Liu, Y. Li, L. Shi, J. Control. Release 329 (2021) 1102–1116.
[6] WHO, Antimicrobial resistance (2021), https://www.who.int/news-room/fact-sheets/detail/antimicrobial-resistance.
[7] M.F. Chellat, L. Raguz, R. Riedl, Angew. Chem. Int. Ed. 55 (2016) 6600–6626.
[8] X. Li, H. Bai, Y. Yang, et al., Adv. Mater. 31 (2019) e1805092.
[9] Y. Wang, Y. Yang, Y. Shi, et al., Adv. Mater. 32 (2020) e1904106.
[10] Y. Ren, H. Liu, X. Liu, et al., Cell Rep. Phys. Sci. 1 (2020) 100245.
[11] L. Mei, S. Zhu, Y. Liu, et al., Chem. Eng. J. 418 (2021) 129431.
[12] G. Qing, X. Zhao, N. Gong, et al., Nat. Commun. 10 (2019) 4336.
[13] T. Yu, G. Jiang, R. Gao, et al., Expert Opin. Drug Deliv. 17 (2020) 1151–1164.
[14] B.M. Luby, C.D. Walsh, G. Zheng, Angew. Chem. Int. Ed. 58 (2019) 2558–2569.
[15] B. Ran, Z. Wang, W. Cai, et al., J. Am. Chem. Soc. 143 (2021) 17891–17909.
[16] J. Li, Z. Meng, Z. Zhuang, et al., Small 18 (2022) e2200743.
[17] H. Zhang, C. He, L. Shen, et al., Chin. Chem. Lett. 34 (2023) 108160.
[18] J. Zuo, E. Zhu, W. Yin, et al., Chem. Sci. 14 (2023) 2139–2148.
[19] T.F. Li, H.Z. Xu, Y.H. Xu, et al., Mol. Pharm. 18 (2021) 3601–3615.
[20] D. Hu, L. Zou, W. Yu, et al., Adv. Sci. 7 (2020) 2000398.
[21] J. Sun, X. Cai, C. Wang, et al., J. Am. Chem. Soc. 143 (2021) 868–878.
[22] P. Xiao, Z. Shen, D. Wang, et al., Adv. Sci. 9 (2022) 2104079.
[23] C.C. Yang, M.H. Tsai, K.Y. Li, et al., Int. J. Mol. Sci. 20 (2019) 2072.
[24] J. Sun, K. Du, J. Diao, et al., Angew. Chem. Int. Ed. 59 (2020) 12122–12128.
[25] Z. Zhuang, J. Dai, M. Yu, et al., Chem. Sci. 11 (2020) 3405–3417.
[26] T.C. Pham, V.N. Nguyen, Y. Choi, et al., Chem. Rev. 121 (2021) 13454–13619.
[27] V.N. Nguyen, Y. Yan, J. Zhao, et al., Acc. Chem. Res. 54 (2021) 207–220.
[28] J.S. Ni, T. Min, Y. Li, et al., Angew. Chem. Int. Ed. 59 (2020) 10179–10185.
[29] H. Fan, Y. Fan, W. Du, et al., Nanoscale 12 (2020) 9517–9523.
[30] W. Li, J. Zhang, Z. Gao, et al., Coordin. Chem. Rev. 471 (2022) 214754.
[31] H.C. Li, X. Tang, S.Y. Yang, et al., Chin. Chem. Lett. 32 (2021) 1245–1248.
[32] J. Roncali, Adv. Energy Mater. 11 (2021) 2102987.
[33] M. Zhang, G. Dai, C. Zheng, et al., Chin. Chem. Lett. 33 (2022) 1110–1115.
[34] I.P. Koskin, C.S. Becker, A.A. Sonina, et al., Adv. Funct. Mater. 31 (2021) 2104638.
[35] B. Zhao, B. Gothe, A. Groh, et al., ACS Appl. Mater. Interfaces 13 (2021) 32461–32466.
[36] O. Gidron, M. Bendikov, Angew. Chem. Int. Ed. 53 (2014) 2546–2555.
[37] S. Li, Q. Deng, Y. Zhang, et al., Adv. Mater. 32 (2020) e2001146.
[38] C. Zhou, J.C.S. Ho, G.W.N. Chia, et al., Adv. Funct. Mater. 30 (2020) 2004068.
[39] M. Yang, H. Zhao, Z. Zhang, et al., Chem. Sci. 12 (2021) 11515–11524.
[40] Z. Zhang, Q. Yuan, M. Li, et al., Small 17 (2021) e2104581.
[41] L. Zhou, F. Lv, L. Liu, et al., CCS Chem. 1 (2019) 97–105.
[42] B. Wang, M. Wang, A. Mikhailovsky, et al., Angew. Chem. Int. Ed. 56 (2017) 5031–5034.
[43] B. Wang, B.N. Queenan, S. Wang, et al., Adv. Mater. 31 (2019) e1806701.
[44] H. Wang, W. Zhao, X. Liu, et al., ACS Appl. Bio Mater. 3 (2019) 593–601.
[45] Z. Zhou, C. Ergene, J.Y. Lee, et al., ACS Appl. Mater. Interfaces 11 (2019) 1896–1906.
[46] C. Du, D. Gao, M. Gao, et al., ACS Appl. Mater. Interfaces 13 (2021) 27955–27962.
[47] K. Wen, H. Tan, Q. Peng, et al., Adv. Mater. 34 (2022) 2108146.